Proceedings of Global Power and Propulsion Society
ISSN-Nr: 2504-4400
GPPS Xi'an21
18th – 20th October, 2021
www.gpps.global

GPPS-TC-2021-0299

Influence of shield on supersonic inlet characteristics

Feichao Cai
School of Power and Energy, Northwestern Polytechnical University
caifeichao@nwpu.edu.cn
Xi'an, Shaanxi，China

Xing Huang
AECC HUNAN AVIATION POWERPLANT RESEARCH INSTITUTE
Huangxing831020@126.com
Zhuzhou, Hunan，China

ABSTRACT

For the supersonic inlet with shield plate, the internal and external flow integration calculation model is established. The influence of shield plate on the flow field parameter distribution of the supersonic inlet is studied by numerical method. The influence of shield plate length on the flow field and inlet performance is analyzed. The influence of shield plate on the aerodynamic performance of the body / inlet with abdominal layout is studied by comparing with the scheme without shield plate The influence of interference. The simulation results show that the shield plate can adjust the shock system configuration of the supersonic inlet and improve the angle of attack characteristics of the inlet. The length of the shield plate has a significant effect on the pre compression effect of the inlet air flow. Adding the shield plate can reduce the interference of the body on the inlet flow field.

INTRODUCTION

Supersonic inlet is an important part of air breathing engine, which has an important influence on engine performance. The flow state of the inlet is complex, and there are complex flow phenomena such as shock/expansion wave system, viscous boundary layer, shock/boundary layer interference, etc. (Julien Weiss et al. 2006, Doyle Knight et al. 2017). The velocity range is from subsonic to supersonic, and it may be disturbed by the flow field outside the body, which challenges the design. With the increasing speed range of aircraft, higher requirements are put forward for inlet design (Dai Chunliang et al. 2019).

Because of its simple structure, fixed geometry inlet has been widely used in small aircraft. However, the change of flight speed and the adjustment of attitude angle will affect the shock system of the inlet, which will affect the performance. On the one hand, the research work of supersonic inlet focuses on improving the performance by flow control, such as local control methods such as boundary layer suction to enhance the total pressure recovery(Wan D et al. 2007, Zhang Hongjun et al. 2008, Soltani M R et al. 2016), or secondary flow injection (Li C et al.2015,Zhao You-xi et al. 2019) to suppress the adverse effects of shock wave/boundary layer; On the other hand, we have carried out a lot of research on inlet regulation technology (Teng Jian et al.2013, Falempin F et al. 2006). By adjusting the structure or aerodynamics, we can change the geometry of the flow passage, such as the compression slope angle of the air flow, the throat height, etc., so as to adjust the compression shock system to adapt to a wider flight state. addition, a lot of research work has been carried out on the aerodynamic and performance interference between the inlet and the external flow field based on numerical simulation or experiment. These research work provides a reference for improving the performance of supersonic inlet.

Compression surface design and shock system organization are the core issues of supersonic inlet design. Although the local flow control method can improve the performance of the inlet, it can not optimize the configuration of shock system. Due to the constraints of space weight and other aspects, the adjustment technology needs to be comprehensively balanced in the application of small-scale aircraft.

1 COMPUTATIONAL MODEL

For the velocity range of ma2 ~ 3.5, the fixed geometry design of three wave system inlet is adopted, and the flow passage is shown in Figure 1. Considering the influence of viscous boundary layer and a certain angle of attack margin, the two-stage compression angle is determined to be 10 degrees. The Mach number of the inlet with the first shock wave seal the inlet is Ma2.8, and the self starting velocity is Ma2.2 under the design condition.

A shield plate is added in front of the inlet, and the length ratio L1/H2 is 0 ~ 2 along the horizontal direction. In order to study the influence of the airframe, an integrated flow field model including the front airframe and the inlet is established. The head of the airframe is parabolic and its diameter is 1.5 times of the height of the inlet, and the width W of the inlet is the same as the height H_2. The main geometric parameters are shown in Table 1.

Table 1 main design parameters geometric parameters

δ (^{0})	10
H_2(mm)	100
W/H_2	1
Φ/H_2	1.5
H_1/H_2	0.5833
$(L_1+L_4)/H_2$	10
L_3/H_2	5

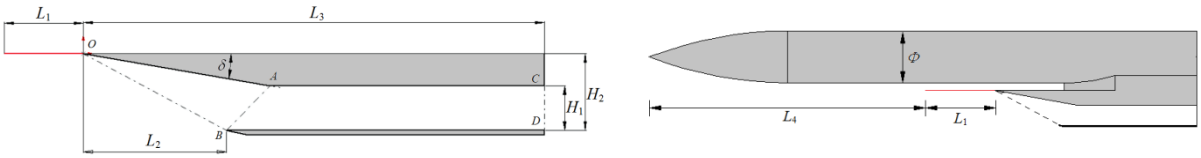

(a) Inlet geometry (b) Body and air inlet

Fig. 1 Calculation Model

2. NUMERICAL MODELING

2.1 MESH GENERATION AND BOUNDARY CONDITIONS

The geometric topology of the inlet is relatively simple, and it can be divided into structured meshes in the process of meshing. Considering the viscous flow and shock / boundary layer flow phenomena, the mesh near the wall is refined.

According to the geometric characteristics of the external flow field, unstructured grids are generated, and the areas near the body surface and the inlet fairing surface are refined. The interface of the internal and external flow field is regarded as the internal surface of the flow, and the grids are naturally transitional. A total of 1.3 million computational grids were generated by grid generation.

The boundary conditions of the model include pressure far field, pressure outlet, wall and symmetry plane. As shown in Figure 2. The windward and side of the computational domain are the pressure far-field boundary , and the pressure, temperature and velocity angle vectors of the incoming flow are specified; Due to the characteristics of supersonic flow, the disturbance propagates unidirectionally. The computational domain of the external field is only taken after the inlet, and the back boundary is the pressure outlet boundary. Given the static pressure and total temperature of the return flow, the outlet of the inlet is also designated as the pressure outlet boundary condition. The wall of the projectile and the inlet are wall boundary, and the heat conduction of the wall is not considered, that is, the wall is adiabatic.

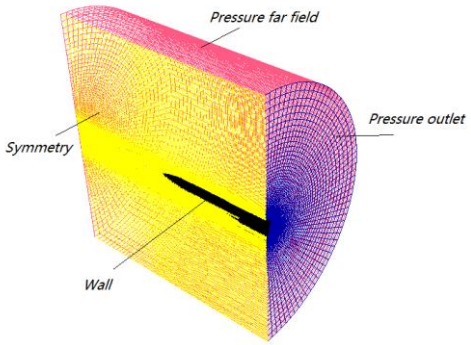

Fig. 2 computational grid and boundary conditions

2.2 CALCULATION STRATEGY

In the process of the operation of the supersonic inlet, the normal shock wave at the end will be generated in the subsonic expansion section under the action of the outlet pressure, and the air flow will be reduced to the subsonic velocity. The whole calculation model including the supersonic compression section, throat section and subsonic

expansion section of the inlet is established. The flow details of the flow field in the inlet can be studied. However, the velocity range in the channel is from ultrasonic to low subsonic, and the interference between the normal shock wave and the boundary layer at the end is serious, and The calculation is difficult and the convergence is poor. The critical working state needs to be iterative repeatedly, and the calculation efficiency is low.

The performance of the inlet depends on the configuration of shock system. During the modeling process, the model takes the outlet position of the equal straight throat section, which is used to evaluate the critical working state of the inlet. The flow in the calculation domain is supersonic flow, and the convergence is good. By numerical calculation, the average distribution of parameters on the exit section CD (Fig. 1) can be obtained directly.

$$\overline{Ma_{th}} = \frac{1}{A}\int MadA = \frac{1}{A}\sum_{i=1}^{n} Ma_i\,|A_i| \tag{1}$$

$$\overline{P_{th}^*} = \frac{1}{A}\int P^* dA = \frac{1}{A}\sum_{i=1}^{n} P^*{}_i\,|A_i| \tag{2}$$

The total pressure recovery of CD section is:

$$\sigma_{th} = \frac{\overline{P_{th}^*}}{P_{00}^*} \tag{3}$$

According to the total pressure loss formula of normal shock wave, the total pressure recovery of normal shock wave under critical working condition is solved:

$$\sigma_N = \frac{1}{\left(\frac{2k}{k+1}Ma_{th}^2 - \frac{k-1}{k+1}\right)^{\frac{1}{k-1}} \left(\frac{2}{k+1}\frac{1}{Ma_{th}^2} - \frac{k-1}{k+1}\right)^{\frac{k}{k-1}}} \tag{4}$$

Considering the influence of viscosity and shock boundary layer interaction, the coefficient K less than 1 is taken as the correction. According to the recommendation of reference(Cai Fei-chao et al.2010), the value is 0.9. The total pressure recovery of the inlet is as follows:

$$\sigma_{Inlet} = K\sigma_{th}\sigma_N \tag{5}$$

According to simulations results, the mass flow of throat $\dot{m}_{\mathrm{th}}$ is obtained. According to the definition, the ratio of $\dot{m}_{\mathrm{th}}$ to free flow captured by the inlet is calculated, which is the flow coefficient:

$$\varphi_{Inlet} = \dot{m}_{\mathrm{th}}/\rho_\infty c_\infty Ma_\infty H_2 W \tag{6}$$

Where ρ_∞ and c_∞ are the density and sound velocity of the incoming flow respectively.

Under the above strategy, the efficiency of simulation calculation is greatly improved.

2.3 COVERNING EQUATIONS AND NUMERIACL SOLUTIONS

The governing equation of the flow field is a weakly conserved Reynolds averaged Navier Stokes equation. On any boundary control body, the conservation equation of scalar φ is written as follows:

$$\frac{d}{dt}\int_V \rho\varphi dV + \int_{\partial V} \rho\varphi\vec{u}\cdot d\vec{A} = \int_{\partial V} \Gamma\nabla\varphi\cdot d\vec{A} + \int_V S_\varphi dV \tag{7}$$

Among them, ρ is fluid density, $\vec{u}$ is velocity vector, Γ is diffusion coefficient and S_φ is source term of φ. Here ∂V is used to represent the boundary of the control body *V*.

Based on the finite volume method, the coupled implicit method is used to solve the governing equations. The diffusion term and convection term in the control equation are discretized by the second-order central difference scheme and the second-order upwind scheme respectively. The $\kappa-\varepsilon$ model is selected for the turbulence model.

2.4 NUMERICAL METHOD VERIFICATION

Using the same numerical modeling method in this paper, including grid division principle, boundary condition setting, numerical solution, turbulence model, etc., the simulation calculation is carried out for the Hyshot model in reference (Reinartz B et al.2003), and compared with the experimental results to study the feasibility of the modeling method. For the calculation grid of 150000 divided by hyshot model, the calculation conditions are consistent with the test conditions, that is, the incoming flow velocity Ma2.5, the total temperature 295k and the total pressure 0.569Mpa.

Comparing the wall pressure calculated by simulation with the test value in Fig. 3, it can be seen that the numerical simulation results are in good agreement with the test results, and the numerical calculation better reflects the position and process of pressure fluctuation caused by shock wave in the inlet.

The Mach number distribution of numerical simulation and test schlieren are compared in Fig. 4. It can be seen that the distribution of the shock wave system obtained by numerical calculation is close to the shock wave system reflected by the test schlieren. The shock wave reflected by the lower lip, the expansion wave at the turning point A of the upper wall, the local separation of the upper wall and the shock wave reflection process in the inner channel can be correctly reflected.

Through the comparison of the above results, it shows that the simulation modeling method in this paper is feasible.

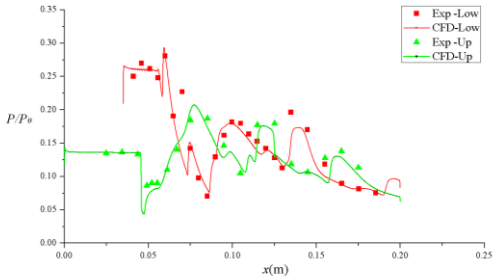

Fig.3 Comparison of wall pressure between experiment and simulation

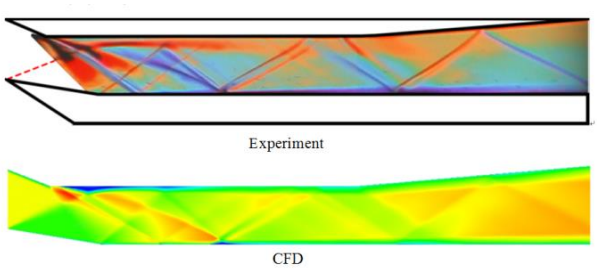

Fig.4 Comparison of Mach number distribution between experimental schlieren and numerical calculation

3. STUDY ON THE INFLUENCE OF PARAMETERS

The flow field parameters and performance of the inlet were analyzed for the self starting speed Ma2.2, shock sealing speed Ma2.8 and cruise speed Ma3.5 respectively.

3.1 FLOW FIELD ANALYSIS OF UNSHIELDED PLATE

For the air inlet without shield plate, the Mach number distribution of flow field under three different flow velocity is compared, as shown in Figure 5.

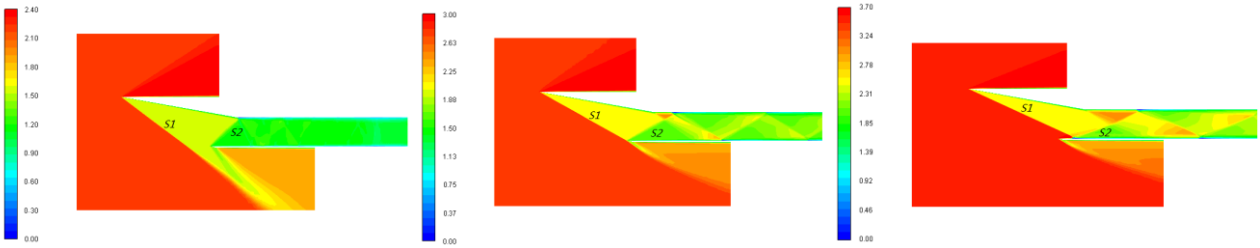

$Ma_{\infty} = 2.2$ $Ma_{\infty} = 2.8$ $Ma_{\infty} = 3.5$

Fig. 5 Mach number distribution at 6 degrees of attack angle

It can be seen that the angle of the first shock S1 is larger and falls outside the lower lip of the inlet when the starting Mach number is Ma2.2. The second shock reflected from the lower lip B (Fig. 1) intersects with the upper wall at the turning point A to form the second oblique shock S2. Then the air flows backward along the horizontal direction, and the Mach number is evenly distributed in the straight section.

At the velocity of Ma2.8, the first oblique shock intersects with the lower wall at the lip B, and the reflected shock S2 is generated. As the velocity increases, the shock angle becomes smaller, and it intersects with the upper wall after the turning point A, and there is a local expansion acceleration region behind the turning point a. In addition, when the shock wave strikes the upper wall, local separation occurs due to the shock/boundary layer interaction, but the separation area is small.

When the inflow velocity increase to Ma3.5, the shock angle of the first shock S1 further decreases and the shock enters into the lip of the lower wall. The local expansion region between the upper wall turning point A and S2 shock wave is larger than that of Ma2.8. The S2 shock wave intersects with the expansion wave and reflects in the straight throat.

The results show that the shock system at self starting Mach number Ma2.2 and the shock sealing state at Ma2.8 are consistent with the design, and the shock system of the inlet will change in a wide velocity range.

3.2 ATTACK ANGLE CHARACTERISTICS OF SHIELD PLATE

Under the condition of zero attack angle, the shield has no effect on the compressed wave system. When the incoming flow has a certain attack angle, the shield plate generates oblique shock wave to the incoming flow compression, which is equivalent to more primary compression inclined plane. The original first stage compression surface of the inlet becomes two-stage compression, and the corresponding angle of attack change relationship is shown in the table below. Obviously, the shield plate pre rectifies the air inlet, and then the air flow flows along the direction of the shield plate to ensure that the compression angle of the compression surface OA (Fig. 3.1) to the air flow is maintained at 10 degrees.

Table 1 equivalent compression angle

Attack angle α	No shield plate (degree)	Shield plate (degree)
0	10+10	0+10+10
6	16+10	6+10+10
12	22+10	12+10+10

Under the above changes, Mach number Ma_{th}, total pressure recovery σ_{th} and inlet total pressure recovery can be calculated by shock wave theory. Based on the shock wave theory, the flow velocity Ma2.8 is taken as an example, and the parameters of the two states are compared in Table 2.

Table 2 Influence of shielding plate on parameters

		$\alpha=0^0$	$\alpha=6^0$	$\alpha=12^0$
Ma_{th}	No shield plate	1.9468	1.6946	1.4074
	Shield plate	1.9468	1.7370	1.5131
σ_{th}	No shield plate	0.9485	0.8797	0.7696
	Shield plate	0.9485	0.9518	0.9180
σ_{Inlet}	No shield plate	0.7073	0.7547	0.7360
	Shield plate	0.7073	0.7996	0.8497

From the above calculation results, the actual compression angle of the first stage compression angle is the superposition of the angle base of the first stage compression surface and the attack angle, and the compression effect of the inlet on the incoming flow is stronger. Compared with the case with shield, the case without shield has lower Mach number Ma_{th}, larger total pressure loss and lower total pressure recovery σ_{Inlet}.

3.3 INFLUENCE OF SHIELD PLATE ON SHOCK WAVE SYSTEM

Taking the velocity Ma2.8 as an example, the Mach number distribution of the flow field with different shield length was compared.

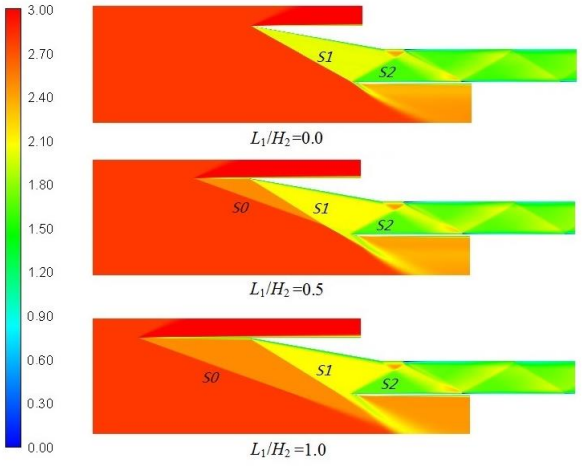

Fig. 6 Mach number distribution of different shield plate length（$\alpha=6^0$）

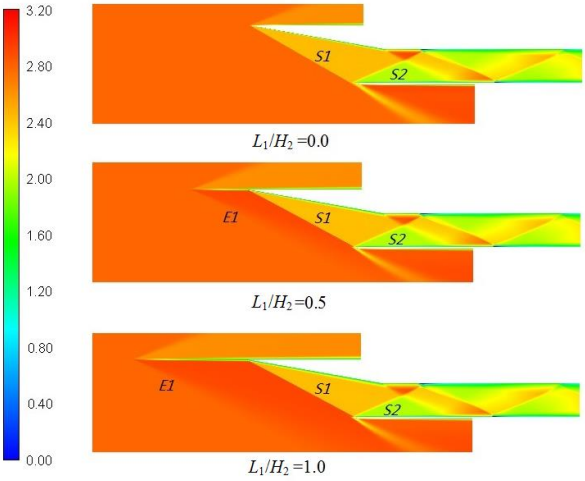

Fig. 7 Mach number distribution of different shield plate length（$\alpha=-3^0$）

Compared with the results at attack angle of 6 degrees(Fig.6), it can be seen that the oblique shock system of the inlet without shield plate is composed of two main shock waves S1 and S2, and the reflection shock system of the straight section. An additional oblique shock S0 is generated at the leading edge of the shield plate after adding the shield plate, and its compression angle to the incoming flow is the attack angle αvalue. After the shock S0 is added, S1 and S2 shock waves are generated by the flow passing through the compression surface of the inlet, as well as the reflection shock wave system in the straight section. Because the velocity behind S1 shock is less than ma2.8, the shock angle increases and S1 shock falls outside the lower lip. When the shield length ratio L1/H2 is 1.0, S0 shock and S1 shock intersect above the lower wall of the inlet; When L1/H2 increases to 2.0, S1 shock falls completely behind S0 shock.

Under the condition of negative angle of attack in Figure 7, when there is no shield plate, the compression angle of the first stage compression surface of the inlet decreases, and the compressibility decreases, and the first shock S1 moves outward slightly beyond the lower lip. The complex reflected shock system is produced by the interference of shock wave and expansion wave in the straight section. When there is a shield plate, the uniformly distributed expansion wave is generated when the air flow bypasses the shielding plate. Due to the increase of air flow velocity, the shock wave angle generated by the first stage compression OA decreases and intersects with the lower wall after the lip point B. By increasing the length of the shield plate, the expansion wave area is enlarged, but the shock wave system in the inlet passage is not affected obviously.

Comparing the inlet outlet parameters at the above attack angle with those in Table 3, it can be seen that at 6 degrees attack angle, with the increase of shield plate length, the Mach number and total pressure of the throat first increase and then decrease, but the change is not obvious when L1/H2 > 1.0. When the attack angle is negative, the throat Mach number and total pressure decrease with the increase of shield length.

Table 3 Comparison of throat parameters

L1/H2	$\alpha = 6^0$		$\alpha = -3^0$	
	Ma_{th}	P^*_{th}	Ma_{th}	P^*_{th}
0.0	1.6922	0.7967	2.0900	0.8486
0.5	1.7132	0.8212	2.0847	0.8327
1.0	1.7344	0.8512	2.0829	0.8204
1.5	1.7362	0.8529	2.0803	0.8134
2.0	1.7344	0.8503	2.0779	0.8094

3.4 INFLUENCE OF SHIELD ON INLET PERFORMANCE PARAMETERS

The performance of inlet with different attack angle and shield length is compared for deferent flight velocity, as shown in Fig. 8 ~ 9.

When the attack angle is less than 6 degrees, the flow coefficient and total pressure recovery coefficient increase with the increase of attack angle. When the attack angle exceeds 6 degrees, the two characteristic parameters show a downward trend. If the attack angle is further increased, the inlet will not start. From the influence of shield length, the value of negative attack angle is less than that without shield, while the value of positive attack angle is greater than that without shield. In addition, when L1 / H2> 1.0, the curves of different plate length basically coincide, indicating that the plate length has no effect on the performance parameters at Ma2.2.

When the velocity increases to Ma2.8, the total pressure recovery begins to decrease when the attack angle of the inlet without shield exceeds 9 degrees, while the total pressure recovery increases significantly at high attack angle when the shield is added. When L1/ H2 > 1.0, the total pressure recovery increases within 15 degrees. The larger the length of shield plate, the smaller the negative attack angle flow coefficient, while the larger the positive attack angle value. When L1/H2 > 1.0, the difference is small.

At high-speed cruise ma3.5 (Fig. 12 and Fig. 13), when the angle of attack increases to 15 degrees without shielding plate, the total pressure recovery and flow coefficient increase, but the increase trend of total pressure recovery decreases, while the flow coefficient increases approximately linearly. At this speed, the negative angle of attack performance decreases while the positive angle of attack performance increases with the increase of the shield plate length, and the total pressure recovery and flow coefficient increase significantly at the positive angle of attack.

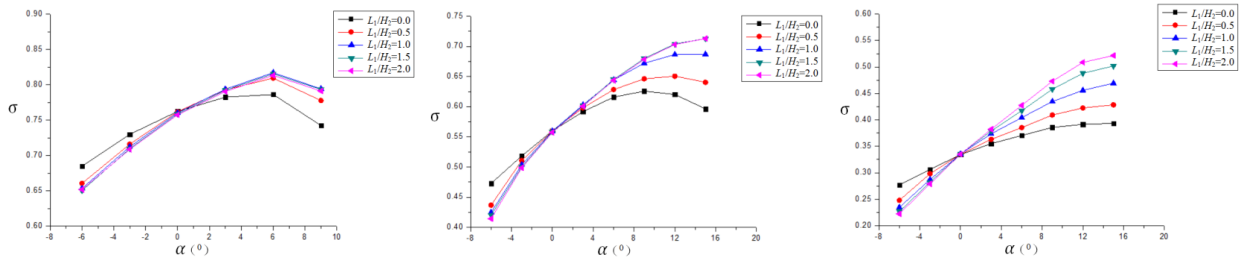

Ma_∞=2.2 Ma_∞=2.8 Ma_∞=3.5

Fig. 8 Variation of total pressure recovery with attack angle

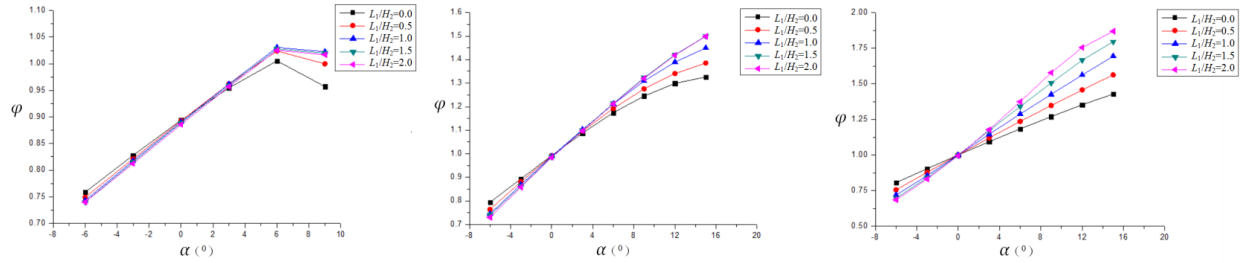

Ma_∞=2.2 Ma_∞=2.8 Ma_∞=3.5

Fig. 9 Variation of flow coefficient with attack angle

3.5 INFLUENCE OF SHIELD PLATE ON INTERFERENCE OF INTERNAL AND EXTERNAL INTERACTION

According to the integrated simulation model of airframe and inlet flow established in this paper, the simulation calculation is carried out under the working conditions of Ma2.8 and 6 degrees of attack angle. The Mach number

distribution in the symmetry plane is shown in Figure 8. It can be seen that when flying at a certain angle of attack, the airframe produces compression effect on the incoming flow, and the inlet is located in the flow field of shock wave interaction between the missile body and the head. When the inlet is far away from the airframe, the influence is reduced.

Figure 9 shows the streamline distribution on the surface of the missile body. It can be seen that the airflow generates a transverse flow from the windward side to the leeward side along the body at the attack angle, which will affect the inlet parameters and flow state. Corresponding to Figure 10, the Mach number distribution of the inlet section is given. A on the left side is in the state of unshielded plate. It can be seen that the Mach number distribution of the inlet section is uneven due to the interference of the body on the front flow, and there are obvious differences in the high speed and low speed regions. On the right side B, the Mach number distribution of the inlet section is increased by increasing the length of L1 / h2 = 1.0 shield plate. Compared with the left side, although the velocity distribution is still uneven, the Mach number difference between the high-speed and low-speed regions is significantly reduced.

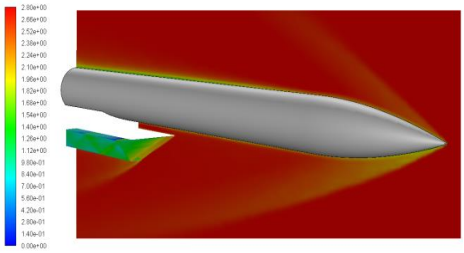

Fig. 10 Mach number distribution in symmetry plane（$\alpha = 6^0$）

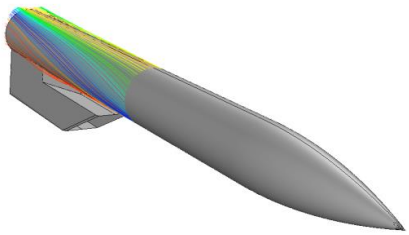

Fig. 11 Flow line of wall area（$\alpha = 6^0$）

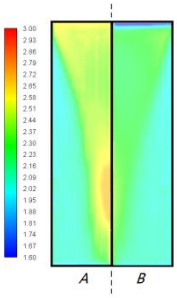

Fig. 12 comparison of Mach number of inlet section（$\alpha = 6^0$）

4. CONCLUSION

For a fixed geometry supersonic two-dimensional inlet, the influence of the shield plate on the flow field parameter distribution and the inlet performance is studied in this paper. According to the simulation results, the main conclusions are as follows:

(1) The shield plate is added in front of the inlet, which is equivalent to the increase of the first compression surface for the flight state of the attack angle, and the number of oblique shock wave system of the inlet, which is beneficial to the performance of the positive attack angle of the inlet. At the same time, the performance of the negative angle of attack will decrease.

(2) The length of the shield plate has an effect on both the flow field and the performance parameters of the inlet. The increase of the shield plate length is beneficial to improve the performance, especially in the high-speed flight conditions, the effect of the length of the shield plate on the total pressure recovery and the flow coefficient is more obvious. However, the increase of plate length will also lead to the increase of structural quality, which needs to be optimized combined with performance parameters.

(3) Under the condition of flight with attack angle, the front body has an effect on the inlet parameters distribution, resulting in the uneven distribution of inlet cross-section parameters. The shield plate can reduce interference of the body on the inlet flow field to a certain extent.

REFERENCES

Julien Weiss，Ndaona Chokani. Quiet Tunnel Experiments of Shockwave/Turbulent Boundary Layer Interaction[R]. AIAA 2006-3362.

Doyle Knight，Mahsa Mortazavi. Hypersonic Shock Wave Transitional Boundary Layer Interactions-A Review[C]. Denver：The 47th AIAA Fluid Dynamics Conference，2017.

Dai Chunliang, Sun Bo, Zhang Kunyuan, Optimization design of the inward turning inlet in the Mach number 3-6 wide velocity domain[J], Journal of Aerospace Power, 2019 34(10),2191~2202

Wan D, Guo R. Experimental Investigation of a Fixed-geometry Two-dimensional Mixed-compression Supersonic Inlet with Sweep-forward High-light and Bleed Slot in an Inverted "X"-type Layout[J]. Chinese Journal of Aeronautics, 2007, 20(4):304-312.

Zhang Hongjun, Xin Xianjun, Bai Kui, Shen Qing, Design and wind tunnel test on supersonic inlet with boundary layer bleed[J], Journal of Experiments in Fluid Mechanics,2008, 22(1): 88-91.

Soltani M R, Daliri A, Younsi J S, et al. Effects of Bleed Position on the Stability of a Supersonic Inlet[J]. Journal of Propulsion & Power, 2016, 32(5):1-14.

Li C, Tan H, Wang D. Influence of Secondary Flow Injection Angle on a Fluidic Shock Control Technique[J]. Journal of Propulsion and Power, 2015, 31(2): 674-684.

Zhao You-xi，Xie Lyu-rong，Wang Kun, et al. A SideWall Flow-Control Method of Supersonic Inlet, Journal of Propulsion Technology, 2019, 40(12): 2673~2682

Teng Jian, Yuan Huacheng, Design methodology of axisymmetric variable geometry inlet[J]. Journal of Aerospace power, 2013, 28(1): 96~103

Falempin F, Wendling E, Goldfeld M, Starov A. Experimental Investigation of Starting Process for a Variable Geometry Air Inlet operating from Mach 2 to Mach 8[R]. AIAA 2006-4513.

Cai Fei-chao, Chen Feng-ming, Xu Dong-lai et al. A fast CFD simulation scheme for supersonic inlet[J]. Joumal of Solid Rocket Technology, 2010,33(1):41~44

Reinartz B, Herrmann C D, Ballmann J, et al. Aerodynamic performance analysis of a hypersonic inlet isolator using computation and experiment[J] .Journal of Propulsion and Power,2003, 19(5) .